AIRFOIL AERODYNAMICS AND AEROACOUSTICS USING COMPRESSIBLE LARGE EDDY SIMULATION

William R. Wolf, willwolf@stanford.edu
João Luiz F. Azevedo, azevedo@iae.cta.br
Instituto de Aeronáutica e Espaço, IAE/DCTA, Brazil

Sanjiva K. Lele, lele@stanford.edu
Department of Aeronautics & Astronautics, Stanford University

Abstract. *The present work concerns the investigation of the broadband noise that arises from the interaction of turbulent boundary layers with an airfoil trailing edge. A compressible large eddy simulation (LES) is conducted for the calculation of nearfield noise sources and farfield acoustic predictions are performed by the Ffowcs Williams-Hawkings (FWH) equation. Flow simulation and acoustic predictions are performed for a NACA0012 airfoil at zero deg. angle of incidence and results are compared to experimental data available in the literature.*

Keywords: *Airfoil noise, LES, Acoustic analogy*

1. INTRODUCTION

The investigation of airfoil noise generation and propagation is of paramount importance for the design of aerodynamic shapes such as wings and high-lift devices, as well as wind turbine blades, fans and propellers. Brooks *et al.* (1989) identify five fundamental airfoil noise mechanisms such as laminar and turbulent boundary layer noise, trailing edge bluntness noise, separation-stall noise and tip vortex noise. The present investigation of airfoil self-noise generation and propagation primarily concerns the broadband noise that arises from the interaction of turbulent and laminar boundary layers with the airfoil trailing edge.

The turbulent aerodynamic flows analyzed give rise to noise sources at a broad range of frequencies and spatial scales. Therefore, large eddy simulation (LES) is the numerical method of choice for the flow simulations since it captures the most energetic scales associated with noise generation at an affordable computational cost compared to direct numerical simulation. The acoustic predictions are performed by the Ffowcs-Williams and Hawkings (1969) (FWH) acoustic analogy formulation. The surface and volume integrations of dipole and quadrupole source terms appearing in the FWH equation are performed using a 3D wideband multi-level adaptive fast multipole method (Wolf and Lele, 2011a,b) (FMM) in order to accelerate the calculations.

Numerical simulations are conducted for a NACA0012 airfoil with tripped boundary layers and rounded trailing edge for zero deg. angle of incidence. The NACA0012 airfoil geometry is chosen due to the large experimental and computational data set available in the literature. The flow Reynolds based on the airfoil chord is fixed at $Re_c = 408000$ and the freestream Mach number is set $M_\infty = 0.115$. In order to validate the current solutions, flow simulation results are compared to experiments by Sagrado and Hynes (2011) and acoustic prediction results are compared to experiments by Brooks *et al.* (1989). Excellent agreement between numerical predictions and experimental data is observed for both aerodynamic and aeroacoustic results.

2. FLOW SIMULATIONS

The general curvilinear form of the compressible Navier Stokes equations is solved using LES. The numerical scheme for spatial discretization is a sixth-order accurate compact scheme (Nagarajan, 2004) implemented on a staggered grid. The current numerical capability allows the use of overset grids with a fourth-order accurate Hermitian interpolation

between grid blocks (Bhaskaran, 2010). The time integration of the fluid equations is carried out by a fully implicit second-order Beam-Warming scheme (Beam and Warming, 1978) in the near-wall region in order to overcome the time step restriction. A third-order Runge-Kutta scheme is used for time advancement of the equations in flow regions far away from solid boundaries. No-slip adiabatic wall boundary conditions are applied along the solid surfaces except for the tripping region where suction and blowing is applied. Characteristic plus sponge boundary conditions are applied in the farfield locations and periodic boundary conditions are applied in the spanwise direction. The dynamic subgrid model formulation of Lilly (1992) is used to include the effects of unresolved turbulent scales. The numerical tool has been previously validated for several compressible flow simulations (Nagarajan, 2004; Bhaskaran, 2010).

3. AEROACOUSTIC PREDICTIONS

The FWH acoustic analogy formulation (Ffowcs-Williams and Hawkings, 1969) is used for the aeroacoustic predictions. In the present work, the surface dipole integrations are computed along the airfoil surface and the volume quadrupole integrations are computed along a subset region of the flowfield including the wake plus turbulent boundary layer regions. These integrations are performed using a 3D wideband multi-level adaptive FMM (Wolf and Lele, 2011a,b) in order to accelerate the calculations of the FWH equation. The developed numerical capability allows the analysis of each noise source individually. Therefore, it is possible to investigate the separate effects of dipole and quadrupole sources. With the method applied in this work the computational cost of the aeroacoustic integrals is considerably reduced.

4. RESULTS

This section discusses aerodynamic and aeroacoustic results obtained by LES and the FWH formulation. In order to validate the present solutions, flow simulation results are compared to experiments by Sagrado and Hynes (2011) and acoustic predictions are compared to experiments by Brooks *et al.* (1989).

The configuration analyzed allows a study of sound generated by turbulent boundary layers convected past the rounded trailing edge of a NACA0012 airfoil at zero deg. angle of incidence. The flow Reynolds number based on the airfoil chord is set $Re_c = 408000$ and the freestream Mach number is $M_\infty = 0.115$. Results are compared to wind tunnel experiments by Sagrado and Hynes (2011). In the experiments, the flow Reynolds number based on the airfoil chord is $Re_c = 400000$, the freestream Mach number is $M_\infty = 0.058$ and the measured freestream turbulence intensity is 0.4%. As one can observe, the Reynolds numbers of numerical simulation and experiments by Sagrado and Hynes (2011) are slightly different. The reason for this is that the flow parameters in the numerical simulation are chosen to exactly match the acoustic wind tunnel experiment from Brooks *et al.* (1989). A trip wire is placed at $x/c = 0.127$ to trip the boundary layers and ensure that they are turbulent at the trailing edge. In the numerical simulations, the boundary layers are tripped by suction over the region $0.15 < x/c < 0.175$ and blowing over the region $0.175 < x/c < 0.20$. The suction and blowing is given by a step function along the span with amplitude $U_{blowing} = U_{suction} = 0.03U_\infty$ chosen from numerical experimentation.

The present grid configuration consists of a symmetric body-fitted O-grid block of size $1536 \times 125 \times 128$ that accurately resolves the turbulent boundary layers close to the airfoil and a Cartesian background grid block of size $896 \times 511 \times 64$ with uniform resolution around the O-grid block and that gently stretches up to the farfield regions. Maximum values of grid spacing in terms of wall units are given by $\Delta x^+ \approx 50$, $\Delta y^+ \approx 0.5$ and $\Delta z^+ \approx 20$. In Fig. 1 (a) one can see iso-surfaces of λ_2 colored by vorticity magnitude along the airfoil region. Both the top and bottom boundary layers present similar behavior and become turbulent at around $x/c = 0.4$. Figure 1 (b) shows iso-surfaces of vorticity magnitude colored by streamwise momentum and a background slice with dilatation contours in gray scale. One can visualize the broad range of scales in the boundary layers and wake, and acoustic field.

In Fig. 2 (a), one can observe a plot of negative pressure coefficient distribution, $-Cp$, along the airfoil chord. The result obtained by LES is compared to a potential flow solution and good agreement is achieved except for the tripping region. The experimental result is also plotted and one can observe the upstream effects of tripping compared to the

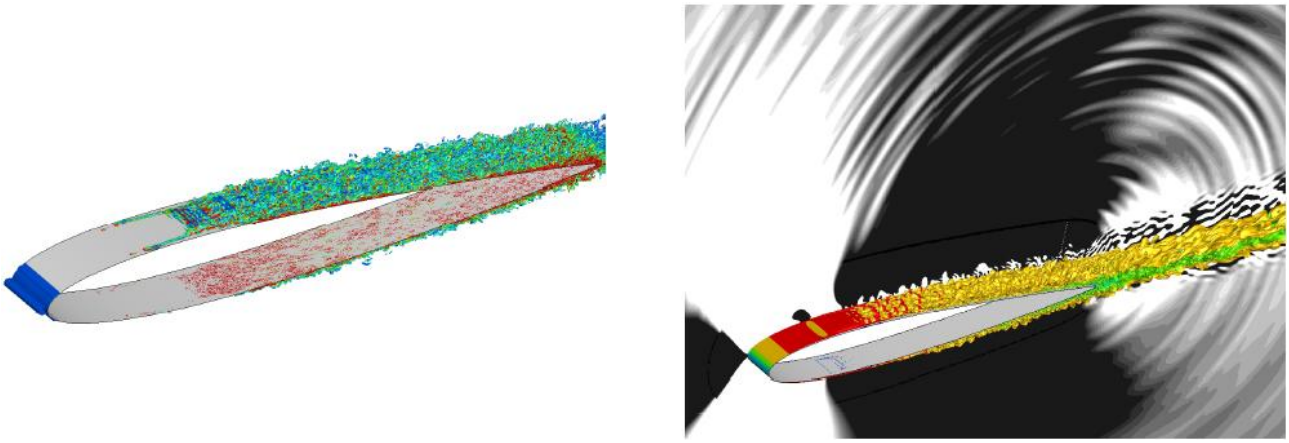

(a) Iso-surfaces of λ_2 colored by vorticity magnitude.

(b) Iso-surfaces of vorticity magnitude colored by streamwise momentum with contours of dilatation in the background.

Figure 1. Large eddy simulation of flow past a NACA0012 airfoil at $\alpha = 0$ deg, $M_\infty = 0.115$ and $Re_c = 408000$.

present LES. Figure 2 (b) shows a comparison in terms of friction coefficient distribution, $C_f = \frac{\tau_w}{1/2\rho U_e}$, along the airfoil chord for the LES and experiments from Sagrado and Hynes (2011). Here, τ_w is the wall shear stress and U_e is the velocity at the edge of the boundary layer. One should notice that the velocity outside the boundary layer varies in the wall normal direction due to curvature of streamlines. The values of C_f obtained from the experimental investigation are provided for the specific locations shown in the plot and excellent agreement is found between the present simulation and experiments. One can observe the increase in C_f after the tripping region where the turbulent boundary layers start developing and the further reduction of C_f downstream towards the trailing edge region.

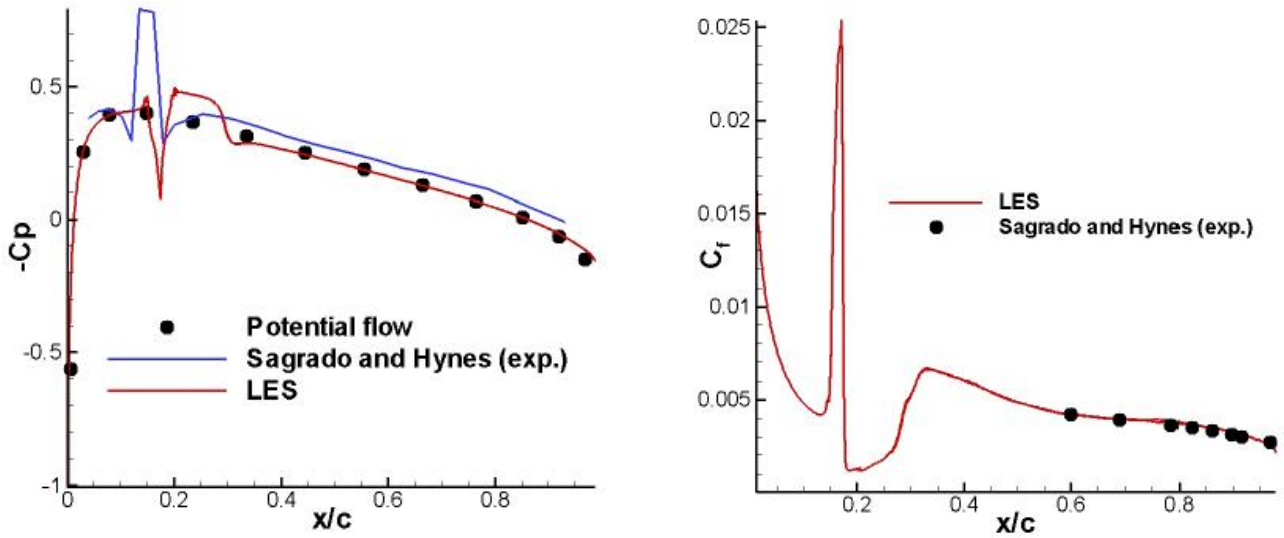

(a) Distribution of $-Cp$ along the airfoil chord.

(b) Distribution of C_f along the airfoil chord.

Figure 2. Flow simulation results.

Figure 3 presents wall pressure power spectral densities normalized by inner variables obtained by LES and experiments at different chord locations. Results normalized with inner variables use τ_ω as the pressure scale and ν/u_τ^2 as the time scale. Good agreement is found between the LES and experimental results for the present normalization. As shown by Gravante *et al.* (1998), the wall pressure spectrum should obey a power-law behavior, $\Phi(\omega) \sim \omega^n$, where n is dependent on the frequency range of the turbulent spectrum. They describe three frequency ranges of the spectrum that exhibit $\Phi(\omega) \sim \omega^{-1}$, $\Phi(\omega) \sim \omega^{-7/3}$ and $\Phi(\omega) \sim \omega^{-5}$. The ω^{-1} and $\omega^{-7/3}$ behaviors are associated with pressure sources in the logarithmic portion of the boundary layer and in the highest portion of the buffer zone, respectively. The ω^{-5} behavior is

associated with sources in the boundary layer below the $y^+ \sim 20$ region. As can be observed in Fig. 3, the ω^{-5} log-law behavior is captured in the LES results. In this figure, one can also see the good agreement between experiment and LES results in terms of frequency range of the wall pressure spectra for the ω^{-5} behavior.

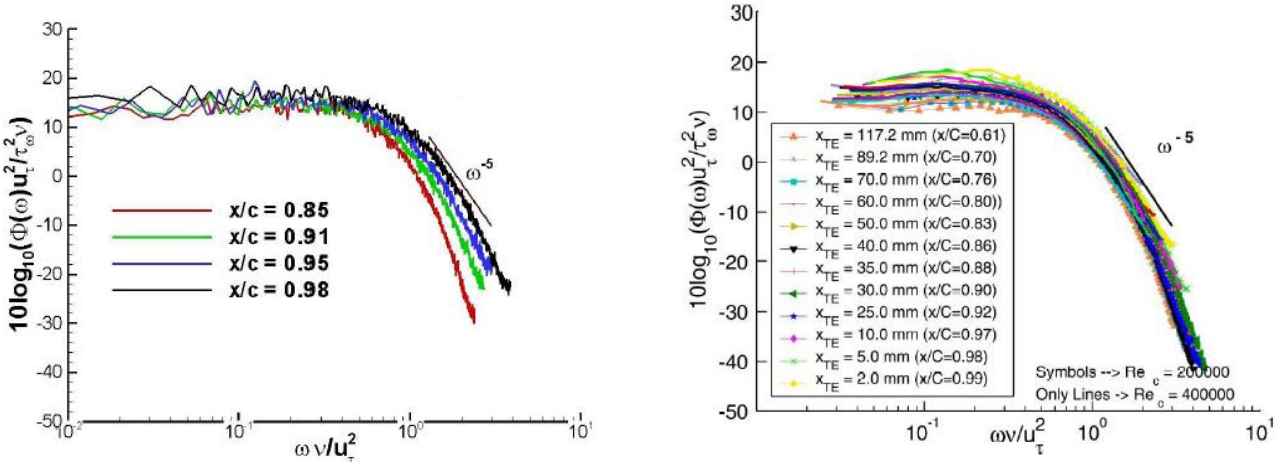

(a) Present LES. (b) Experiments from Sagrado and Hynes (2011).

Figure 3. Wall pressure power spectral densities normalized by inner variables at different chord locations.

The FWH acoustic analogy formulation is used to predict the farfield sound generated by the airfoil and the present large eddy simulation provides the near flowfield used to compute the acoustic source terms that are transformed to the frequency domain. Dipole source integrations are computed along the airfoil surface and quadrupole source integrations are computed along the airfoil and wake regions. The frequency domain source terms are computed from 1024 time samples divided in three segments of 512 records with 50% overlap. Numerical results are compared to experimental data by Brooks *et al.* (1989). In the experiment, the flow Reynolds number based on the airfoil chord is $Re_c = 408000$, the freestream Mach number is $M_\infty = 0.115$ and the measured freestream turbulence intensity is less than 0.05%. The spanwise width is three times the chord length, $Lz_{exp} = 3c$. A random distribution of grit in strips is used from the leading edge to $x/c = 0.2$ to trip the boundary layers. The commercial grit number used was 60 and the density of particles was 380 $particles/cm^2$

In the present LES, the spanwise width is $Lz_{LES} = 0.1c$ and, therefore, the ratio $Lz_{exp}/Lz_{LES} = 30$. An assessment of the spanwise coherence is necessary to predict the frequency spectrum of the sound pressure radiated by the full span width. The pressure spanwise coherence is defined as

$$\gamma^2(z, \Delta z, f) = \frac{|\Phi_{pp}(z, \Delta z, f)|^2}{|\Phi_{pp}(z, 0, f)||\Phi_{pp}(z + \Delta z, 0, f)|}, \tag{1}$$

where the cross spectrum function Φ_{pp} is the Fourier transform of the space-time cross correlation function

$$\Phi_{pp}(z, \Delta z, f) = \int_{-\infty}^{\infty} \langle p(z, t)p(z + \Delta z, t + \tau)\rangle e^{-if\tau} d\tau. \tag{2}$$

Figure 4 (a) shows the spanwise coherence of the surface pressure on the upper surface of the airfoil at $x/c = 0.95$ for three different Helmholtz numbers. As one can notice, the coherence drops considerably for all frequencies and source regions separated by Lz_{LES} radiate sound independently from neighboring sources in a statistical sense. Therefore, the total noise spectrum is computed as the sum of contributions from Lz_{exp}/Lz_{LES} independent source regions along the span (Wang and Moin, 2000). In Fig. 4 (b), one can observe a comparison of sound pressure level between the current prediction and experiment for a microphone positioned at $x = c$, $y = 7.9c$ and $z = 0.05c$. The effects of convection and non-linear sources are also shown in the figure. The present numerical predictions show good agreement with the experimental measurements. Non-linear quadrupole sources have negligible effect on the total SPL at all frequencies for

the present flow Mach number. However, despite the low freestream Mach number, convection effects are important for the SPL predictions, specially at mid and high-frequencies.

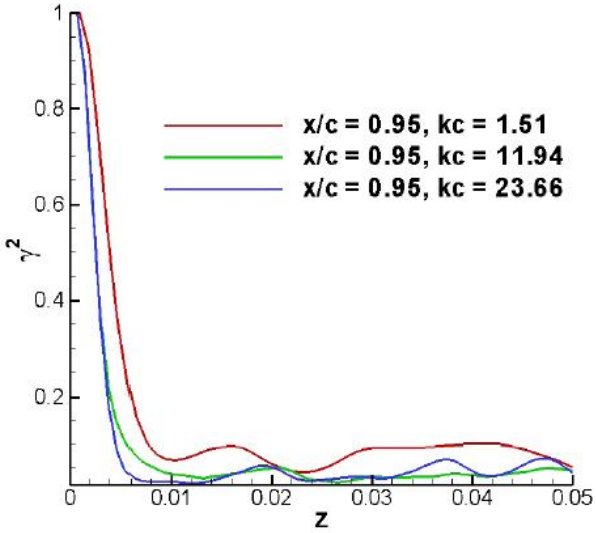

(a) Spanwise coherence of the surface pressure on the upper surface of the airfoil at $x/c = 0.95$.

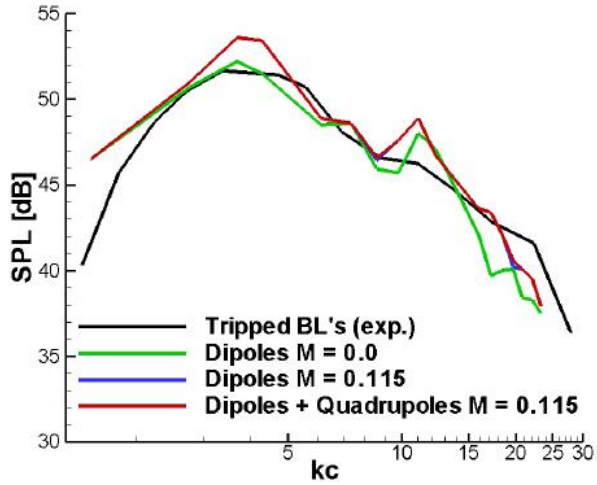

(b) Sound pressure level at observer location $x = c$, $y = 7.9c$ and $z = 0.05c$.

Figure 4. Aeroacoustic prediction results for configuration 1.

In Fig. 5, one can observe the directivity plots for different frequencies measured at observer locations at mid-span and $7.9c$ distant from the airfoil trailing edge. In this figure, one can also see the acoustic fields computed by the FMM-FWH formulation. Dipole and quadrupole sources are included for both directivity and field plots. Significant differences due to convection effects can be observed in the directivity plots, specially for upstream lobes at high frequencies. For compact sources with Helmholtz numbers $kc < 2\pi$, dipole directivities typical of the free-space Green's function (Curle, 1955) are observed (Figs. 5 (a) and (b)) and for non-compact sources, $kc > 2\pi$, directivities resemble the typical cardioid pattern of the half-space Green's function (Ffowcs-Williams and Hall, 1970) (Figs. 5 (c) and (d)). One should see that the airfoil has a finite chord and the ideal cardioid directivity expected for the half-plane problem is not expected since scattering effects occur at the airfoil leading edge. One can also see in Fig. 5 the initial increase in acoustic pressure magnitude for the lower frequencies followed by a decrease of pressure magnitude for higher frequencies, similarly to the SPL plot shown in Fig. 4 (b). For the present simulation, the computational cost reduction factors obtained by the FMM-FWH method range from ≈ 3 for calculations of directivity plots including only dipole sources to ≈ 100 for field solutions with dipoles. These factors are computed for the highest frequency analyzed. Higher cost reduction factors are obtained at lower frequencies. Cost reduction factors are also increased for calculations of quadrupole source terms.

5. CONCLUSIONS

The present investigation of airfoil trailing edge noise generation and propagation concerns the broadband noise that arises from the interaction of turbulent boundary layers with the airfoil trailing edge. A large eddy simulation (LES) is conducted for a NACA0012 airfoil with rounded trailing edge for a flow configuration with Reynolds number based on the airfoil chord fixed at 408000 and freestream Mach number $M_\infty = 0.115$. The acoustic predictions are performed by the Ffowcs Williams & Hawkings (FWH) acoustic analogy formulation and incorporate convective effects. Surface and volume integrations of dipole and quadrupole source terms appearing in the FWH equation are performed using a 3D wideband multi-level adaptive fast multipole method (FMM) in order to accelerate the calculations of aeroacoustic integrals.

For the configuration investigated, boundary layer tripping is applied on the top and bottom sides of the airfoil and turbulent boundary layers develop along both walls. Broadband surface pressure spectra generated by the turbulent boundary

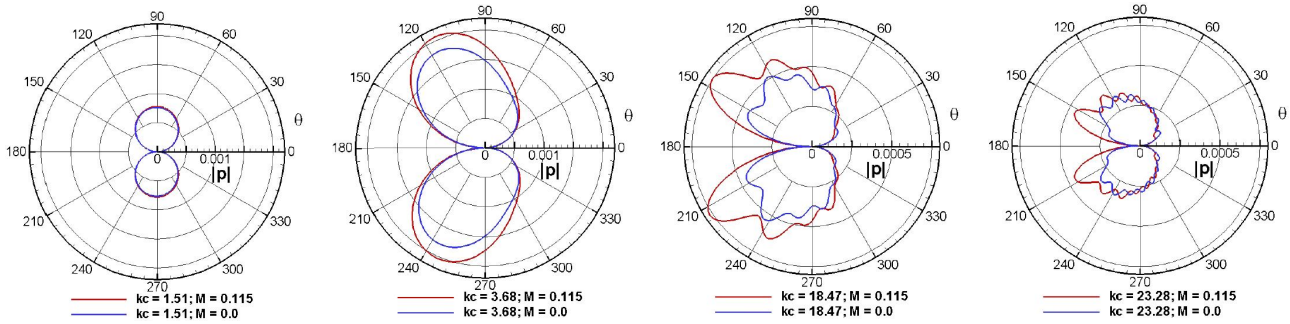

(a) Directivity plot for $kc = 1.51$. (b) Directivity plot for $kc = 3.68$. (c) Directivity plot for $kc = 18.47$. (d) Directivity plot for $kc = 23.28$.

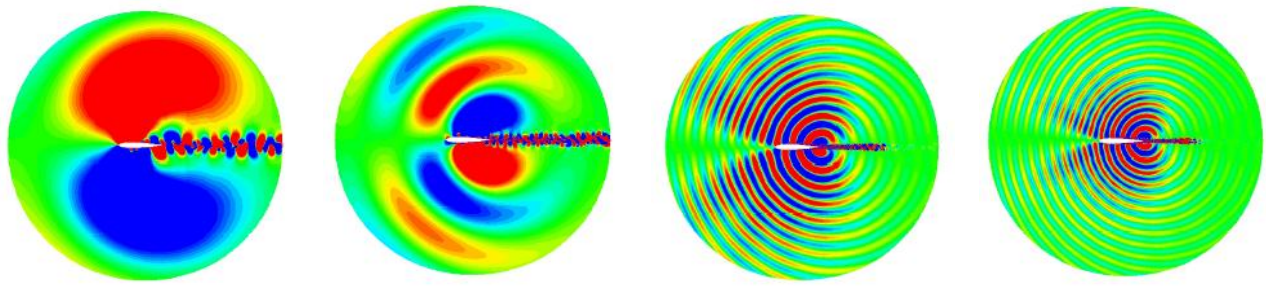

(e) Acoustic near field for $kc = 1.51$. (f) Acoustic near field for $kc = 3.68$. (g) Acoustic near field for $kc = 18.47$. (h) Acoustic near field for $kc = 23.28$.

Figure 5. Aeroacoustic prediction results.

layers are observed in the numerical simulations. Non-linear quadrupole noise sources have negligible effect on farfield sound radiation for the present freestream Mach number. Hence, accurate aeroacoustic predictions can be obtained by surface acoustic pressure data. Despite the low Mach number, mean flow effects are important for the SPL predictions, especially at mid and high-frequencies, for upstream observer locations. Excellent agreement is found between values of wall pressure power spectral density computed by LES and those measured in experiment. Aeroacoustic predictions of sound pressure level also present very good agreement compared to experimental data.

6. ACKNOWLEDGEMENTS

The authors acknowledge the financial support received from FAPESP under Grant No. 2011/12493-6, and from CNPq under Grants No. 312064/2006-3 and No. 471592/2011-0. The computational resources provided by the National Science Foundation are also gratefully acknowledged. The authors further acknowledge the following award for providing computing resources that have contributed to the research results reported within this paper: MRI-R2: Acquisition of a Hybrid CPU/GPU and Visualization Cluster for Multidisciplinary Studies in Transport Physics with Uncertainty Quantification. Finally, the authors also kindly acknowledge the financial support received from GE during the initial stages of the present work.

7. REFERENCES

Beam, R.M. and Warming, R.F., 1978. "An implicit factored scheme for the compressible navier-stokes equations". *AIAA Journal*, Vol. 16, pp. 393–402.

Bhaskaran, R., 2010. *Large Eddy Simulation of High Pressure Turbine Cascade*. Ph.D. thesis, Stanford University, Stanford.

Brooks, T.F., Pope, D.S. and Marcolini, M.A., 1989. "Airfoil self-noise and prediction". NASA Reference Publication 1218.

Curle, N., 1955. "The influence of solid boundaries upon aerodynamic sound". *Proceedings of the Royal Society A*, Vol. 231, pp. 505–514.

Ffowcs-Williams, J.E. and Hall, L.H., 1970. "Aerodynamic sound generation by turbulent flow in the vicinity of a scattering half plane". *Journal of Fluid Mechanics*, Vol. 40, pp. 657–670.

Ffowcs-Williams, J.E. and Hawkings, D.L., 1969. "Sound generation by turbulence and surface in arbitrary motion". *Philosophical Transaction of the Royal Society of London, Series A, Mathematical and Physical Sciences*, Vol. 264, pp. 321–342.

Gravante, S.P., Naguib, A.M., Wark, C.E. and Nagib, H.M., 1998. "Characterization of the pressure fluctuations under a fully developed turbulent boundary layer". *AIAA Journal*, Vol. 36, pp. 1808–1816.

Lilly, D.K., 1992. "A proposed modification of the germano subgrid-scale closure method". *Physics of Fluids*, Vol. 4, pp. 633–635.

Nagarajan, S., 2004. *Leading Edge Effects in Bypass Transition*. Ph.D. thesis, Stanford University, Stanford.

Sagrado, A.G. and Hynes, T., 2011. "Wall pressure sources near an airfoil trailing edge under turbulent boundary layers". *Fluids and Structures - under review*.

Wang, M. and Moin, P., 2000. "Computation of trailing-edge flow and noise using large-eddy simulation". *AIAA Journal*, Vol. 38, pp. 2201–2209.

Wolf, W.R. and Lele, S.K., 2011a. "Aeroacoustic integrals accelerated by fast multipole method". *AIAA Journal*, Vol. 49, pp. 2274–2285.

Wolf, W.R. and Lele, S.K., 2011b. "Wideband fast multipole boundary element method: Application to acoustic scattering from aerodynamic bodies". *International Journal for Numerical Methods in Fluids*, Vol. 67, pp. 2108–2129.

8. RESPONSIBILITY NOTICE

The authors are the only responsible for the printed material included in this paper.